Intraoperative Fully Automatic Registration of Fluoroscopic Image Pair: Cadaveric Evaluation

Sandeep[1*], Vishwanath Reddy B[1*], Abhilash Chakkaravarthy[1*], Vivek Maik[1], Aparna Purayath[1], Suhail Ansari T. A.[1], Manojkumar Lakshmanan[1], and Mohanasankar Sivaprakasam[2†]

[1] Healthcare Technology Innovation Centre, IIT Madras, India
[2] Indian Institute of Technology (IIT) Madras, India
mohan@ee.iitm.ac.in

Abstract. Pedicle screw placement remains a challenge in minimally invasive spine surgery (MISS), largely because mobile C-Arms lack pre-acquisition geometric calibration and exhibit position-dependent imaging distortion. In this paper, we propose a fully automatic 2D C-Arm fluoroscopic image registration system that requires only an anterior-posterior (AP) and lateral (LA) image with overlaid fiducial markers from a custom-designed calibration drum, a rigid frame attached to the C-Arm with metal sphere fiducials distributed across two non-coplanar planes. The framework performs automatic fiducial detection, distortion correction, and camera calibration. Evaluated on phantom, cadaveric, and patient data, the pipeline achieves sub-pixel reprojection error (RPE) and clinically acceptable accuracy, yielding Grades A and B on the Gertzbein-Robbins (GR) scale.

Keywords: Fluoroscopic calibration · Intraoperative registration · Pedicle screw navigation · Image-guided surgery · Device-agnostic deployment · Cadaveric validation

1 Introduction

Pedicle screw placement in MISS is a highly precision-demanding procedure, where even a slight trajectory deviation can lead to serious spinal injuries or nerve root damage [17,2]. Mobile C-Arm fluoroscopy remains the dominant intraoperative modality for MISS [5,13]. Without a CT modality, C-Arm fluoroscopy alone is responsible for guiding the MISS pedicle placement [14]. The AP and LA shots need to be registered to the intraoperative patient anatomy for the MISS surgery to be accurate [15]. This can be achieved using calibration methods such as: (i) *Manual methods* [11,19], where the surgeon manually clicks fiducial points in every image. This method is often time-consuming, causing a 5–15 min delay per case. (ii) *Device-specific methods* [10,3] that rely on factory

*Equal contribution
†Corresponding author

distortion maps or isocentric C-Arm geometry, making them incompatible with the diverse range of C-Arm models from different manufacturers. (iii) *Learning-based methods* [8,7] that achieve sub-pixel landmark localisation but require large C-Arm-specific training sets and offer no mathematical guarantees on geometric accuracy. In this paper, we address the above-mentioned drawbacks with a five-stage fully automatic pipeline anchored to a Coordinate Measuring Machine (CMM) characterised multi-faceted calibration drum, which can be deployed on any C-Arm unit without any hardware/software modifications.

2 Methodology

The proposed pipeline is organized into five sequential stages (Fig. 2). Captured AP and LA fluoroscopic images are preprocessed and passed to blob detection, where candidates are filtered and distortion-corrected to yield undistorted centroids. These centroids are labeled using the known drum geometry to establish 2D–3D correspondences for projection matrix estimation, which is subsequently used for real-time tool projection.

2.1 Multi-Faceted Calibration Drum

Fig. 1. Custom-designed multi-faceted calibration drum.

The proposed pipeline uses a multi-faceted calibration drum as shown in Fig. 1 with metallic spherical fiducials embedded. The ground truth of the calibration drum is derived from the 3D positions of its fiducial markers measured by a CMM, which directly determines the baseline accuracy. The dual-plane fiducial configuration of the drum ensures a geometrically stable estimation of the projection matrix. The drum consists of calibration fiducials for 2D-3D correspondences, distortion fiducials for evaluating and removing the distortion, and positional fiducials for angular reference during fiducial labeling. The fiducials are arranged in a dual-plane layout which provides the required depth variation that a single-plane design [3] lacks, enabling accurate estimation of both intrinsic and extrinsic camera parameters. The multi-faceted design ensures that IR

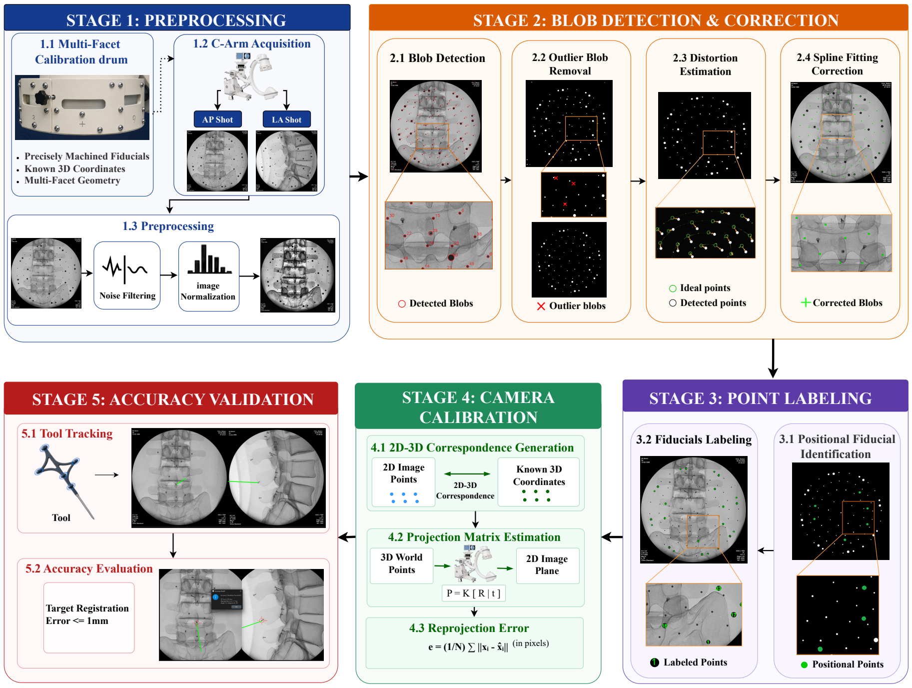

Fig. 2. The fully automatic device-agnostic registration pipeline. Processing flows left-to-right through preprocessing and distortion correction (top), then right-to-left through point labeling, calibration, and validation.

markers on the drum are visible to the camera, irrespective of the drum's side, for reliable tracking in all orientations.

2.2 Fiducial Detection

The C-Arm-captured image is first pre-processed for contrast enhancement and noise removal, after which the fiducial detection module [16] identifies the fiducials based on size, circularity, and convexity, rejecting noise artifacts and elongated anatomical structures. Each fiducial undergoes contour-based shape verification to minimise false positives, and images with insufficient fiducials are rejected.

2.3 Distortion Correction

C-Arm fluoroscopy typically exhibits geometric distortions, including pincushion and S-distortion [18], which cause fiducial markers to appear displaced from their true locations. Detected fiducials are clustered by Euclidean distance to identify the four concentric rings and map them to their actual positions on

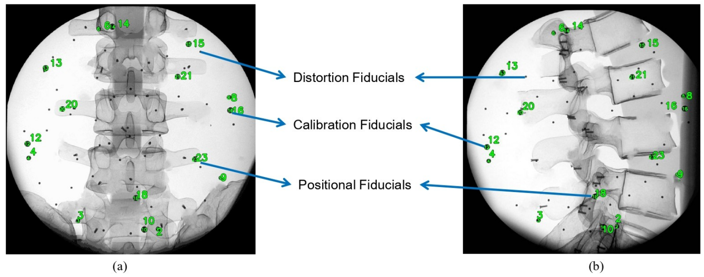

Fig. 3. Automatic fiducial labeling on (a) AP and (b) LA views. Arrows mark the three fiducial categories: *Distortion*, *Calibration*, and *Positional*.

the calibration drum. Because imaging magnification varies with C-Arm zoom and source-to-detector distance, a millimeter-to-pixel scale factor is estimated for each image by minimizing the cumulative radial alignment error between detected and true ring positions. Each fiducial is matched to its ideal undistorted position to establish an optimal one-to-one correspondence. These correspondences are then used to drive an iterative thin-plate spline (TPS) warp, computing the corrected positions.

2.4 Fiducial Labeling

After distortion correction, each fiducial must be ordered sequentially to establish fiducial-to-CMM correspondence for the projection matrix computation. The detected fiducials are separated into their respective planes by clustering radial distance from the image center, yielding distinct ring groups. Each ring group is ordered by comparing the angular positions of each fiducial to positional fiducials and matching against a pre-computed angular reference [4], leading to the ordering of the calibration fiducials as shown in Fig. 3.

2.5 Camera Calibration

Correspondences are established between the ordered 2D fiducial points and the known 3D CMM points. Using the Direct Linear Transform (DLT) [1,9] and Levenberg-Marquardt refinement, the 3×4 projection matrix $\mathbf{P} = \mathbf{K}[\mathbf{R} \mid \mathbf{t}]$ is computed. The resulting projection matrices support intraoperative MISS across all acquired views with consistent sub-pixel RPE. The estimated projection matrix is then validated by projecting the optically tracked tool tip from patent reference space to AP and LA image space and computing the TRE against known ground truth position.

3 Experimental Results

To fully assess geometric accuracy and clinical feasibility, experiments included: (i) a controlled phantom study to determine baseline geometric accuracy; (ii) a

Table 1. Performance of fiducial detection in the C++ pipeline against MATLAB benchmark, using 564 heterogeneous fluoroscopic images (phantom and cadaveric). The calibration drum includes 86 physical fiducials.

Implementation	**Mean ± Std**	**Min**	**Max**	**Reg Time Taken**
MATLAB	91.54 ± 17.67	26	132	6.4 sec
C++	87.82 ± 16.20	17	181	0.8 sec
Ground Truth (Drum)	86	—	—	—

cadaveric study with pedicle screw placement; and (iii) an evaluation of live patient data to assess algorithmic performance under surgical setups. All cadaveric and patient studies were approved by the institutional ethics committee, and informed consent was obtained from all participants.

3.1 Blob Detection Reliability

Achieving accurate 2D-2D registration crucially depends on precisely locating the calibration drum's fiducials prior to estimating its camera matrix. We evaluated our fiducial detection module by performing blob detection on a large and diverse dataset of **564** fluoroscopic images, including both phantom and cadaveric scans. Table 1 reports the detected fiducial counts obtained using the proposed C++ and Matlab builds. Both implementations consistently exceeded the 86-fiducial ground truth (calibration 17 + distortion 64 + positional 5) of the calibration drum. The false positives due to anatomical structures and intensifier artifacts are subsequently discarded during outlier removal in the distortion correction stage, ensuring only valid drum fiducials are retained for calibration.

3.2 Phantom Study

Experiments were performed on Sawbones lumbar spine phantom models in a controlled operating theater setup as shown in Fig. 4. To establish the ground-truth spatial relationship, an optical tracking camera was used to capture the real-time transformations from the camera to the patient reference marker (PRM) ($\mathbf{T}_{\mathrm{PRM}}^{\mathrm{CAM}}$) rigidly attached to the phantom, from the camera to the calibration drum IR markers ($\mathbf{T}_{\mathrm{CD}}^{\mathrm{CAM}}$), and from the camera to surgical tool markers ($\mathbf{T}_{\mathrm{Tool}}^{\mathrm{CAM}}$) used to mark the target location on spinal vertebrae as illustrated in Fig. 5. The spatial relationship between the C-Arm image space and the patient reference space was established during image acquisition via a transformation that maps the calibration drum coordinate frame to the patient reference frame through the camera frame.

$$\mathbf{T}_{\mathrm{PRM}}^{\mathrm{CD}} = (\mathbf{T}_{\mathrm{CD}}^{\mathrm{CAM}})^{-1} \cdot \mathbf{T}_{\mathrm{PRM}}^{\mathrm{CAM}}, \tag{1}$$

This transformation, combined with the independently estimated AP and LA projection matrices, maps both views into a common patient coordinate frame, enabling registered tool overlay on both images.

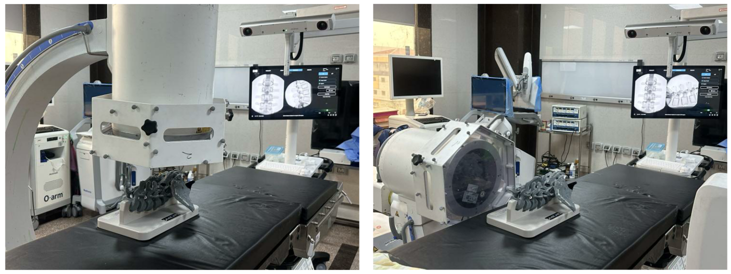

(a) (b)

Fig. 4. Experimental setups. (a) Anteroposterior (AP) C-Arm setup. (b) Lateral C-Arm setup.

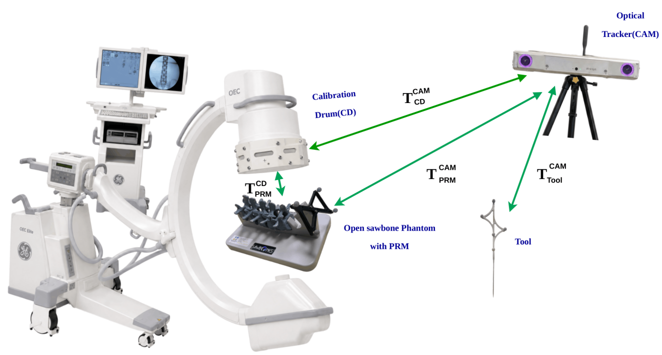

Fig. 5. Tracking setup illustrating the optical tracking camera, patient reference frame, calibration drum, and a surgical tool with the associated coordinate transformations.

Finally, to overlay the tracked tool onto the 2D fluoroscopic images, the tool tip 3D coordinates were projected into image space using the estimated projection matrix from the calibration stage. Experiments on open Sawbones phantoms were conducted across five scenarios, varying the distance between the phantom and the calibration drum from 130 mm to 250 mm for AP views and from 250 mm to 320 mm for LA views. The results are presented in Table 2.

3.3 Cadaveric Study

To validate clinical feasibility under realistic surgical conditions, we conducted a cadaveric evaluation spanning two specimens and two surgical techniques as illustrated in Figure 6. Each specimen was instrumented at multiple thoracic and lumbar levels under both open and MISS approaches. Two user groups participated: surgeons with prior navigated experience (Group 1) and surgeons

Table 2. Registration Accuracy — Open Sawbones

Scenario	AP Dist.	LA Dist.	Mean 3D Error (mm)	Std. Dev. (mm)	95% CI (mm)
1	130 mm	320 mm	0.80	0.33	1.46
2	150 mm	350 mm	0.94	0.33	1.61
3	200 mm	300 mm	0.73	0.29	1.31
4	150 mm	200 mm	0.81	0.36	1.52
5	200 mm	250 mm	1.20	0.33	1.85
Mean			**0.90**	**0.33**	**1.55**

without prior experience (Group 2). All screws were independently graded post-operatively by CT using the GR scale [6], where Grade A (0 mm breach) and Grade B (<2 mm breach) are considered clinically acceptable. Across both specimens and all navigation arms, **94%** of all screws placed were clinically acceptable (Grade A or B). The proposed pipeline achieves a **90.47%** acceptance rate compared to landmark-based registration which achieved **96.5%**. Figure 7 summarizes the GR grade distribution by registration method and surgical technique, demonstrating that the proposed pipeline achieves clinical accuracy comparable to the conventional landmark-based approach, while eliminating the need for pre-operative CT scanning and time-consuming manual landmark-based registration intraoperatively.

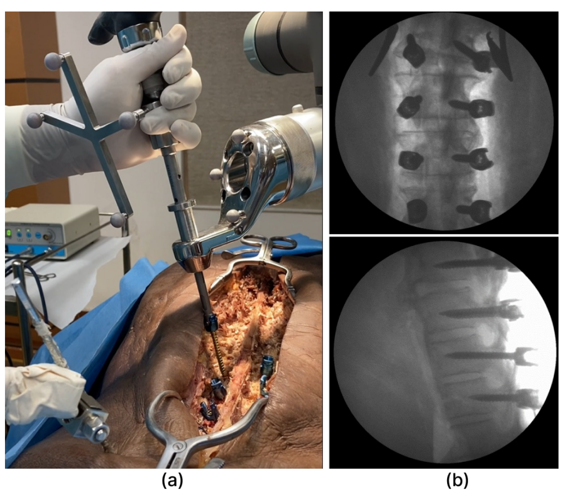

Fig. 6. Cadaveric study setup and verification. (a) Open procedure setup. (b) Intraoperative lateral and AP fluoroscopic views.

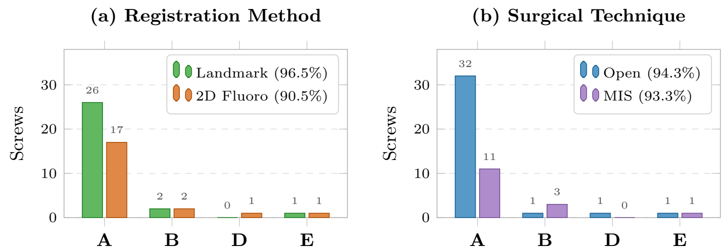

GR Grade key: A = 0 mm breach; B < 2 mm; D < 6 mm; E > 6 mm

Fig. 7. GR-grade screw distribution from the cadaveric study (50 screws total, both user groups). (a) 2D fluoroscopic registration achieves 90.5% Grade A+B acceptance, closely matching landmark (96.5%). (b) Open (94.3%) and MISS (93.3%) arms perform equivalently, validating the pipeline under both surgical approaches.

Table 3. Summary of ongoing patient trials data (As of 20-June-2026)

Metric	Overall Summary	Deformity Cases	Non-deformity Cases
Total Cases	7	4	3
Total Screws	25	16	9
Screw Distribution by Anatomy			
Cervical	0	0	0
Thoracic	2	0	2
Lumbar	15	10	5
Sacrum	8	6	2

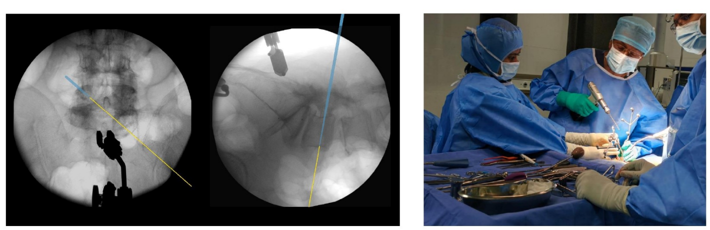

(a) (b)

Fig. 8. Ongoing patient trials setup. (a) Real-time tool tracking interface. (b) Surgical site during a live clinical case.

3.4 Patient Trials

In order to further validate the proposed system in a clinical environment, patient trials were conducted on 7 patients, comprising 4 deformity and 3 non-deformity cases. In total, 25 pedicle screws have been placed using the proposed registration. Table 3 shows the overall composition of the patient cases along with their respective screw implantation rates in various spinal anatomy categories [12].

4 Conclusion and Future Work

In this paper, we proposed a fully automatic, device-agnostic 2D fluoroscopic image registration system anchored by a multi-faceted calibration drum with non-coplanar fiducials and a fiducial detection pipeline. Phantom and cadaveric validations demonstrated that the pipeline achieves clinically acceptable registration accuracy, with a TRE below the 1 mm threshold required for accurate pedicle screw placement. Future work will focus on deep learning and template matching-based fiducial recovery to address detection failures, along with large-scale patient trials for comprehensive clinical validation.

Disclosure of Interests. The authors have no competing interests.

References

1. Abdel-Aziz, Y.I., Karara, H.M.: Direct linear transformation from comparator coordinates into object space coordinates in close-range photogrammetry. Photogrammetric Engineering and Remote Sensing **81**(2), 103–107 (1971), reprinted in PE&RS, 2015
2. Ansari, T.A.S., Maik, V., Naheem, M., Ram, K., Lakshmanan, M., Sivaprakasam, M.: A hybrid-layered system for image-guided navigation and robot-assisted spine surgeries. In: 2024 IEEE/SICE International Symposium on System Integration (SII). p. 1452–1457. IEEE (Jan 2024). https://doi.org/10.1109/sii58957.2024.10417647, http://dx.doi.org/10.1109/SII58957.2024.10417647
3. Bertelsen, A., Garin-Muga, A., Echeverría, M., Gómez, E., Borro, D.: Distortion correction and calibration of intra-operative spine X-ray images using a constrained DLT algorithm. Computerized Medical Imaging and Graphics **38**(7), 558–568 (2014). https://doi.org/10.1016/j.compmedimag.2014.06.006
4. Besl, P.J., McKay, N.D.: A method for registration of 3-D shapes. IEEE Transactions on Pattern Analysis and Machine Intelligence **14**(2), 239–256 (1992). https://doi.org/10.1109/34.121791
5. Bott, O.J., Dresing, K., Wagner, M., Raab, B.W., Teistler, M.: Informatics in radiology: use of a C-arm fluoroscopy simulator to support orthopedic surgical training. RadioGraphics **31**(3), E65–E75 (2011). https://doi.org/10.1148/rg.313105125
6. Gertzbein, S.D., Robbins, S.E.: Accuracy of pedicular screw placement in vivo. Spine **15**, 11–14 (1990), https://api.semanticscholar.org/CorpusID:26123791
7. Gopalakrishnan, V., Dey, N., Golland, P.: Intraoperative 2d/3d image registration via differentiable x-ray rendering. In: 2024 IEEE/CVF Conference on Computer Vision and Pattern Recognition (CVPR). pp. 11662–11672 (2024). https://doi.org/10.1109/CVPR52733.2024.01108
8. Grupp, R.B., Unberath, M., Gao, C., Hegeman, R.A., Murphy, R.J., Alexander, C.P., Otake, Y., McArthur, B.A., Armand, M., Taylor, R.H.: Automatic annotation of hip anatomy in fluoroscopy for robust and efficient 2D/3D registration. International Journal of Computer Assisted Radiology and Surgery **15**(5), 759–769 (2020). https://doi.org/10.1007/s11548-020-02162-7
9. Hartley, R., Zisserman, A.: Multiple View Geometry in Computer Vision. Cambridge University Press, 2nd edn. (2003)

10. Heemeyer, F., Choudhary, A., Desai, J.P.: Pose-aware C-arm calibration and image distortion correction for guidewire tracking and image reconstruction. In: 2020 International Symposium on Medical Robotics (ISMR). pp. 181–187 (2020). https://doi.org/10.1109/ISMR48346.2020.9312953
11. Livyatan, H., Yaniv, Z., Joskowicz, L.: Gradient-based 2-D/3-D rigid registration of fluoroscopic X-ray to CT. IEEE Transactions on Medical Imaging **22**(11), 1395–1406 (2003). https://doi.org/10.1109/TMI.2003.819288
12. Maik, V., Purayath, A., R, D., Lakshmanan, M., Sivaprakasam, M.: Gui-based pedicle screw planning on fluoroscopic images utilizing vertebral segmentation. In: 2024 IEEE International Symposium on Medical Measurements and Applications (MeMeA). pp. 1–6 (2024). https://doi.org/10.1109/MeMeA60663.2024.10596889
13. Markelj, P., Tomaževič, D., Likar, B., Pernuš, F.: A review of 3D/2D registration methods for image-guided interventions. Medical Image Analysis **16**(3), 642–661 (2012). https://doi.org/10.1016/j.media.2010.03.005
14. P, Y.R., S, G., R, D., Purayath, A., Maik, V., Lakshmanan, M., Sivaprakasam, M.: Spine vision – x-ray image based gui planning of pedicle screws using enhanced yolov5 for vertebrae segmentation. In: 2024 46th Annual International Conference of the IEEE Engineering in Medicine and Biology Society (EMBC). pp. 1–6 (2024). https://doi.org/10.1109/EMBC53108.2024.10781813
15. Parthasarathy, S., R, D., N, V., Maik, V., Purayath, A., Lakshmanan, M., Sivaprakasam, M.: Enpro: Enhancing precision through optimization in image-guided spine surgical procedures. In: Drechsler, K., Oyarzun Laura, C., Freiman, M., Chen, Y., Wesarg, S., Erdt, M. (eds.) Clinical Image-Based Procedures. pp. 42–52. Springer Nature Switzerland, Cham (2024)
16. Purayath, A., Maik, V., Chakkaravarthy, A., Lakshmanan, M., Sivaprakasam, M.: A novel Spatio^2-Frequency blob detection algorithm for enhancing precision in image guided surgery. In: 2024 IEEE International Symposium on Medical Measurements and Applications (MeMeA). pp. 1–6. IEEE (2024). https://doi.org/10.1109/MeMeA60663.2024.10596825
17. Sommer, F., Goldberg, J.L., McGrath, J.L., Kirnaz, S., Medary, B., Härtl, R.: Image guidance in spinal surgery: a critical appraisal and future directions. International Journal of Spine Surgery **15**(s2), S74–S86 (2021). https://doi.org/10.14444/8137
18. Yaniv, Z., Joskowicz, L.: Long bone panoramas from fluoroscopic X-ray images. IEEE Transactions on Medical Imaging **23**(1), 26–35 (2004). https://doi.org/10.1109/TMI.2003.819923
19. Zheng, G., Zhang, X.: Robust automatic detection and removal of fiducial projections in fluoroscopy images: an integrated solution. Medical Engineering & Physics **31**(5), 571–580 (2009). https://doi.org/10.1016/j.medengphy.2008.11.009